Interferometry imaging for the evolving source in heavy ion collisions at HIRFL-CSR energy*

YIN Hong-Jie(尹洪杰)[1] M. J. Efaaf[1] ZHANG Wei-Ning(张卫宁)[1,2,3;1)]

[1] School of Physics and Optoelectronic Technology, Dalian University of Technology, Dalian 116024, China
[2] Department of Physics, Harbin Institute of Technology, Harbin 150006, China
[3] Center of Theoretical Nuclear Physics, National Laboratory of Heavy Ion Accelerator of Lanzhou, Lanzhou 730000, China

Abstract: Imaging analysis of two-pion interferometry is performed for an evolving particle-emitting source in heavy ion collisions at HIRFL-CSR energy. The source evolution is described by the relativistic hydrodynamics in (2+1) dimensions. The model-independent characteristic quantities of the source are investigated and compared with the interferometry results obtained by the usual Gaussian formula fit. It is found that the first-order source function moments can describe the source sizes. The ratio of the normalized standard deviation $\widetilde{\sigma}$ to the first-order moment $\widetilde{R}$, $\widetilde{\sigma}/\widetilde{R}$, is sensitive to the shape of the source function.

Key words: interferometry, imaging, evolving sources, heavy ion collisions, HIRFL-CSR energy

PACS: 25.75.-q, 25.75.Gz **DOI:** 10.1088/1674-1137/36/3/005

1 Introduction

The Cooling Storage Ring (CSR) is an accelerator at the Heavy Ion Research Facility in Lanzhou (HIRFL). The bombarding energy of the HIRFL-CSR for heavy ion collisions will reach about 1 GeV. At this energy nuclei are fully stopped in the center-of-mass frame of the nuclear system in central collisions, and baryon densities may reach 2–3 times normal nuclear matter density ($\sim$0.17 fm^{-3}).

In Ref. [1], the interferometry technique of quantum transport of interfering pair (QTIP) [2] is used for the spherical pion-emitting source in the collisions at HIRFL-CSR energy. However, more realistic sources in the collisions are anisotropic in longitudinal (beam direction) and transverse directions. A cylindric source along the beam direction is a more general case. In Ref. [3], the three-dimension source characteristic quantities $\widetilde{R}_{\rm out}$, $\widetilde{R}_{\rm side}$, and $\widetilde{R}_{\rm long}$ obtained by an interferometry imaging technique are investigated for granular sources in relativistic heavy ion collisions. In this work we perform imaging analysis for the cylindric evolving sources in heavy ion collisions at the HIRFL-CSR energy. We investigate the source characteristic quantities obtained by the imaging analysis and the interferometry results obtained by the usual Gaussian formula fit for the evolving source. The results indicate that the first-order source moments $\widetilde{R}_{\rm out}$, $\widetilde{R}_{\rm side}$, and $\widetilde{R}_{\rm long}$ can describe the source sizes, and the zero-order moment $\widetilde{\lambda}$ may provide information on the chaotic degree of the source. Unlike the interferometry results obtained by the usual Gaussian formula fit, the results of the moments are model independent. The ratio of the normalized standard deviation to the first-order moment is sensitive to the shape of the source function. Its results are larger than unity for the source function with a non-Gaussian distribution.

2 (2+1) dimension evolving sources

2.1 Relativistic hydrodynamic equations in cylindric frame

Relativistic hydrodynamics has been extensively applied to high energy heavy ion collisions [4–7]. In this work we use the relativistic hydrodynamics in (2+1) dimensions to describe the source evolution.

Received 10 May 2011
* Supported by National Natural Science Foundation of China (11075027)
1) E-mail: wnzhang@dlut.edu.cn

The dynamics of an ideal fluid in high energy heavy ion collisions is defined by the local conservations of energy-momentum and net charges [4–6]. The continuity equations of the conservations of energy-momentum, net baryon number, and entropy are

$$\partial_\mu T^{\mu\nu}(x) = 0, \quad (1)$$

$$\partial_\mu j_{\rm b}^\mu(x) = 0, \quad (2)$$

$$\partial_\mu j_{\rm s}^\mu(x) = 0, \quad (3)$$

where x is the space-time coordinate of a thermalized fluid element in the source center-of-mass frame, $T^{\mu\nu}(x)$ is the energy momentum tensor of the element, $j_{\rm b}^\mu(x) = n_{\rm b}(x)u^\mu$ and $j_{\rm s}^\mu(x) = s(x)u^\mu$ are the four-current-density of baryon and entropy, ($n_{\rm b}$ and s are the baryon density and entropy density), and $u^\mu = \gamma(1, \boldsymbol{v})$ is the four-velocity of the fluid element. The energy momentum tensor $T^{\mu\nu}(x)$ is given by [4–6]

$$T^{\mu\nu}(x) = \left[\epsilon(x) + P(x)\right] u^\mu(x) u^\nu(x) - P(x) g^{\mu\nu}, \quad (4)$$

where P and ϵ are the pressure and energy density of the fluid element, and $g^{\mu\nu}$ is the metric tensor.

In the cylindrical coordinate (t, ρ, ϕ, z) frame, $g^{\mu\nu}=$ diag $(1, -1, -\rho^{-2}, -1)$. The conservation Eqs. (1)–(3) can be expressed as

$$\partial_t E + \partial_\rho[(E+P)v^\rho] + \partial_z[(E+P)v^z] = -\frac{v^\rho}{\rho}(E+P), \quad (5)$$

$$\partial_t M^\rho + \partial_\rho(M^\rho v^\rho + P) + \partial_z(M^\rho v^z) = -\frac{v^\rho}{\rho} M^\rho, \quad (6)$$

$$\partial_t M^z + \partial_\rho(M^z v^\rho) + \partial_z(M^z v^z + P) = -\frac{v^\rho}{\rho} M^z, \quad (7)$$

$$\partial_t N_{\rm b} + \partial_\rho(N_{\rm b} v^\rho) + \partial_z(N_{\rm b} v^z) = -\frac{v^\rho}{\rho} N_{\rm b}, \quad (8)$$

$$\partial_t N_{\rm s} + \partial_\rho(N_{\rm s} v^\rho) + \partial_z(N_{\rm s} v^z) = -\frac{v^\rho}{\rho} N_{\rm s}, \quad (9)$$

where $E \equiv T^{00}$, $M^\rho \equiv T^{0\rho} = T^{\rho 0}$, $M^z \equiv T^{0z} = T^{z0}$, $N_{\rm b} \equiv j_{\rm b}^0 = n_{\rm b}\gamma$, $N_{\rm s} \equiv j_{\rm s}^0 = s\gamma$. Eqs. (5)–(9) are the equations of motion in our model.

2.2 Equation of state and the initial condition

In the equations of motion (5)–(9), there are ϵ, P, v^ρ, v^z, $n_{\rm b}$, and s six unknown functions. In order to obtain the solution of the equations of motion, we need an equation of state (EOS), $P(\epsilon,\, n_{\rm b},\, s)$, which gives a relation for P, ϵ, $n_{\rm b}$, and s. Also, the initial conditions of the source system are needed for the solution. At the HIRFL-CSR energy the particle-emitting source is a system of mixed hadronic gas with finite baryon density. In our model, we use a mixed perfect gas of (N, π, K) (stable particles) and Δ(1232) (excited-state particles) to describe the hadronic gas source as in Refs. [1, 2]. We assume that the initial source is distributed uniformly in a cylinder along the z axis (in beam direction) between $(-z_0, z_0)$ and with a transverse radius ρ_0. The initial source has a constant baryon chemical potential $\mu_{\rm b0}$ (or density $n_{\rm b0}$) and zero velocity because of the fully stopped collisions. We assume that the final pion production satisfies the partial chemical equilibrium (PCE) condition [1, 2, 8, 9], which includes the direct pion emission at the chemical freeze-out with temperature $T_{\rm ch}$ and the decayed pion production from $\Delta \to \pi + {\rm N}$ between the chemical freeze-out and thermal freeze-out [1, 2].

For the PCE condition, there is [1, 2, 8, 9]

$$\frac{\bar{n}_i(T, \mu_i)}{s(T, \mu_1, \mu_2, \cdots)} = \frac{\bar{n}_i(T_{\rm ch}, \mu_i^{\rm ch})}{s(T_{\rm ch}, \mu_1, \mu_2, \cdots)}, \quad (i = 1, 2, \cdots), \quad (10)$$

where temperature T is between the chemical freeze-out temperature $T_{\rm ch}$ and the thermal freeze-out temperature $T_{\rm th}$, μ_i is the chemical potential of the species i, $\bar{n}_i = n_i + \sum_{j\neq i} \tilde{d}_{j\to i} n_j$, $\tilde{d}_{j\to i}$ is the fraction of the stable particle species i to which the exited-state particle species j decays. From Eq. (10) one can get the chemical potentials of the particles at $T_{\rm ch} > T > T_{\rm th}$, and then obtain the EOS with the thermodynamic equations of the particle number density n_i, energy density ϵ, pressure P, and entropy density s. Some details about the EOS and PCE condition may be found in Refs. [1, 2].

As in Ref. [1], in our calculations the initial temperature and baryon chemical potential are taken to be $T_0 = 100$ MeV and $\mu_{\rm b0} = 810$ MeV, which correspond to an initial energy density of $\epsilon_0 = 0.47$ GeV/fm^3 and a baryon density of $n_{\rm b0} = 0.42$ fm^{-3}. The chemical freeze-out temperature is taken to be $T_{\rm ch} = 76$ MeV, and the corresponding chemical potential is 830 MeV. They are consistent with the extrapolations obtained from hadronic abundances at CERN/SPS, NBL/AGS, and GSI/SIS [10, 11] collision energies. Based on the criteria of the dependance of thermal freeze-out temperature to the system energy density [12] at finite baryon chemical potential, the thermal freeze-out temperature is chosen as $T_{\rm th} = 40$ MeV, which corresponds to a thermal freeze-out energy density $\epsilon = 47$ MeV/fm^3 close to 45 MeV/fm^3 predicted in Ref. [12].

2.3 Numerical solution

After knowing the EOS and initial conditions we can solve the equations of motion (5)–(9) numerically by the HLLE scheme [4, 5, 7, 13–15].

In Fig. 1, we show the two-dimension density of the energy in the x-z plane, $\epsilon(x,z)=\int\epsilon(x,y,z)\mathrm{d}y$. Here the initial transverse and longitudinal sizes of the (2+1) hydrodynamic source are taken to be $\rho_0 = z_0 = 5$ fm. One can see that energy density decreases rapidly with time. At $t = 10$ fm/c, the energy density at the center of the source is about half the initial energy density at the center. Figs. 2(a) and (b) show the average transverse velocity $\langle v_\rho(\rho)\rangle_z=\int v_\rho(\rho,z)\mathrm{d}z$ and the average longitudinal velocity $\langle v_z(z)\rangle_\rho=\int v_z(\rho,z)\mathrm{d}\rho$ as functions of the transverse and longitudinal coordinates, respectively.

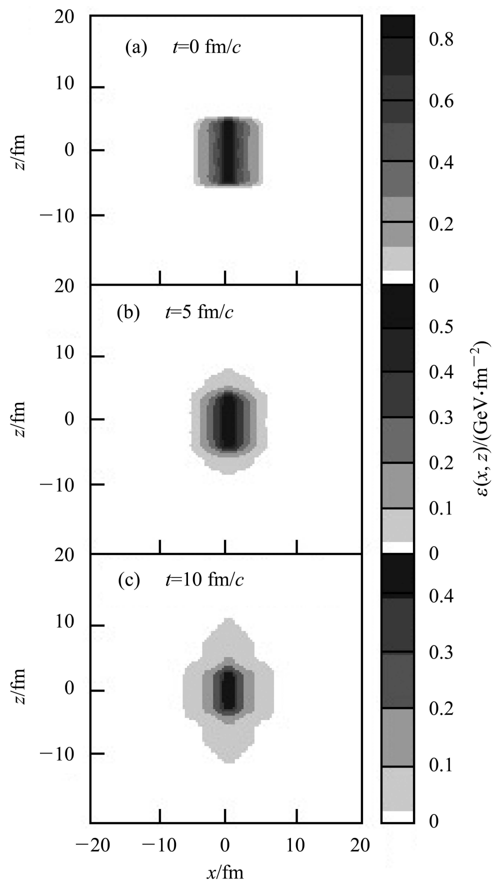

Fig. 1. Two-dimensional density of energy in x-z plane for the (2+1) hydrodynamic source with $\rho_0 = z_0 = 5$ fm.

3 Two-pion interferometry results

Two-pion interferometry (Hanbury-Brown-Twiss effect) has been widely used in high-energy heavy-ion collisions to provide information on the space-time structure of a particle-emitting source [16, 17]. The correlation function $C(k_1,\ k_2)$ of HBT interferometry is defined as the ratio of the two-particle momentum distribution $P(k_1,\ k_2)$ to the the product of the single-particle momentum distribution $P(k_1)P(k_2)$. Using the QTIP interferometry technique [2], one can calculate the single-pion and two-pion momentum distributions numerically, and construct the HBT correlation function for the evolving sources [1, 2].

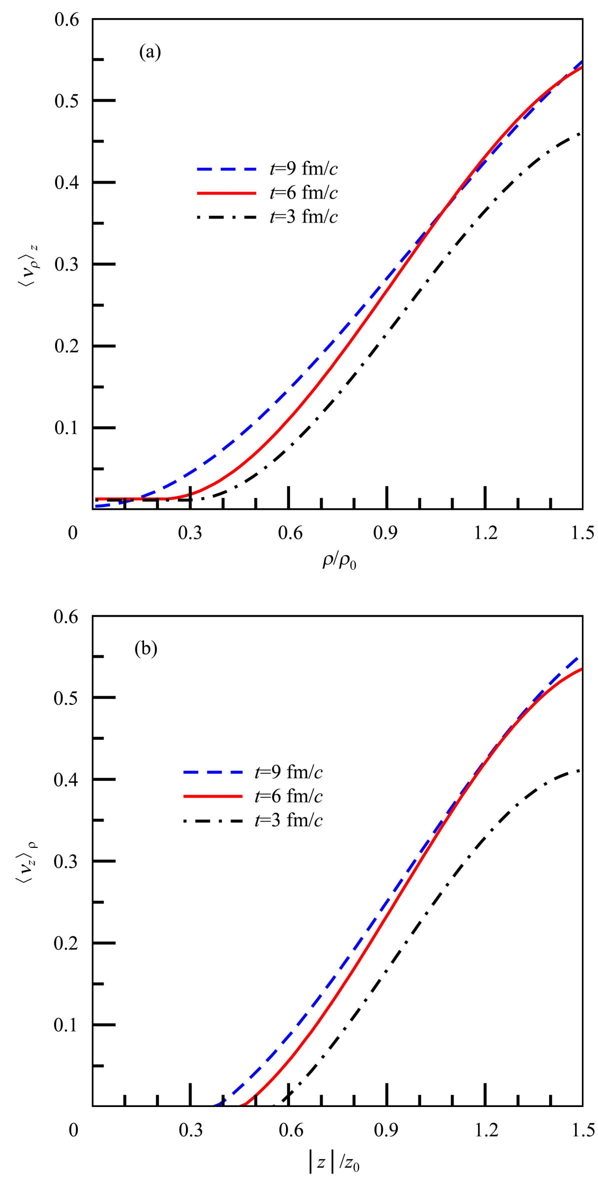

Fig. 2. (a) The average transverse velocity over coordinate z. (b) The average longitudinal velocity over coordinate ρ.

The imaging technique introduced by Brown and Danielewicz [18] allows one to obtain the two-pion source function $S(r)$, the probability for emitting a pion pair with spatial separation r in the pair center-of-mass system (PCMS), from the HBT correlation function. For our (2+1) dimension evolving source, we use the three-dimension imaging method [19] to obtain the source functions $S(r_x)$, $S(r_y)$, and $S(r_z)$ [3, 20], in the 'out' (parallel to the transverse momentum of pion pair $\boldsymbol{k}_{\rm T}=(\boldsymbol{k}_{1\rm T}+\boldsymbol{k}_{2\rm T})/2$), 'side' (in the transverse plane and perpendicular to $\boldsymbol{k}_{\rm T}$), and 'long' (along z axis) directions [21].

Figure 3(a), (b), and (c) show the source functions $S(r_x)$, $S(r_y)$, and $S(r_z)$ for the larger and smaller transverse momenta of the pion pair $k_{\rm T}$. Here the axis label r_j denotes r_x, r_y, and r_z for the panels (a), (b), and (c), respectively. It can be seen that the source function in the out direction is wider than that in the side direction, and has a long tail at larger $k_{\rm T}$. This reflects the fact that the source expansion, which boosts the pair momentum, leads to different geometries in the out and side directions. The shape of the source function with the long tail is very different from that of the Gaussian source [3, 22]. For the larger $k_{\rm T}$, the width of the source function in the out direction is larger than that for the smaller $k_{\rm T}$. However, the width of the source function in the side direction is smaller at larger $k_{\rm T}$ than that at smaller $k_{\rm T}$. The source function width in the long direction is smaller at larger $k_{\rm T}$ because the average longitudinal momentum of the pairs is smaller at larger $k_{\rm T}$.

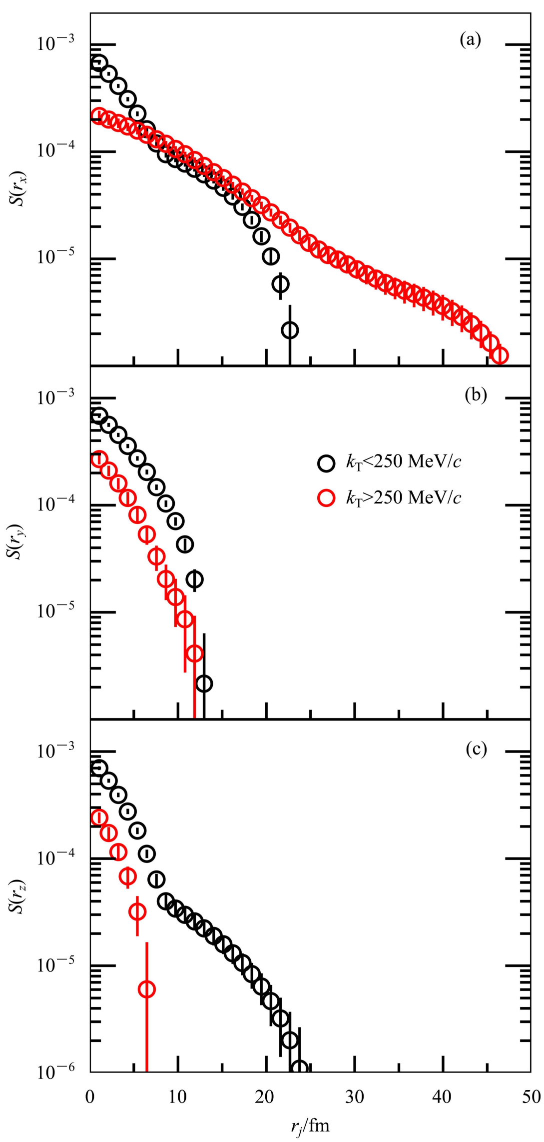

Fig. 3. The source functions in x(out), y(side), and z(long) directions.

Once the source functions $S(r_i)$ are obtained, we can calculate the moments $\langle r_i^n\rangle$ $(n=1,2,\ldots)$ of r_i for the source functions, which provide the quantitative information of the sources. The normalized first-order moment and standard deviation, which are normalized to the Gaussian radius $R_{\rm g}$ for a one dimensional Gaussian source $[S(r_i)\sim\exp(r_i^2/4R_{\rm g})]$, are defined as [3]

$$\widetilde{R}_i=\frac{\sqrt{\pi}}{2}\langle r_i\rangle, \tag{11}$$

$$\widetilde{\sigma}_i=\frac{\sqrt{\langle r_i^2\rangle-\langle r_i\rangle^2}}{\sqrt{2-4/\pi}}, \tag{12}$$

where $i=x,y,z$, and

$$\langle r_i^n\rangle=\frac{\int{\rm d}r_i r_i^n S(r_i)}{\int{\rm d}r_i S(r_i)},\quad n=1,2,\ldots \tag{13}$$

It is demonstrated in Ref. [3] that the quantities $\widetilde{R}_i$ are suitable for describing the source sizes, and the ratio $\widetilde{\sigma}_i/\widetilde{R}_i$ reflects the deviation of the source distribution from the Gaussian form Ref. [3]. Figs. 4(a), 4(b), and 4(c) show the moments $\widetilde{R}_i$ (symbols $\triangle$) calculated for our model source as functions of $k_{\rm T}$ in the out, side, and long directions, respectively. In Figs. 4(e), 4(f), 4(h), we exhibit the usual HBT radii for the source, $R_{\rm out}$, $R_{\rm side}$, and $R_{\rm long}$, obtained by fitting the HBT correlation function with the Gaussian parameterized formula

$$C(q_{\rm out},q_{\rm side},q_{\rm long})=1+\lambda{\rm e}^{-q_{\rm out}^2R_{\rm out}^2-q_{\rm side}^2R_{\rm side}^2-q_{\rm long}^2R_{\rm long}^2}. \tag{14}$$

Here $q_{\rm out}$, $q_{\rm side}$, and $q_{\rm long}$ are the components of the relative momentum of the pion pair in the out, side, and long directions, and in the longitudinally comoving system (LCMS) [17]. In Fig. 4(a), the symbols $\triangledown$ denote the results of $\widetilde{R}'_x=\gamma_{\rm T}^{-1}\widetilde{R}_x$, where $\gamma_{\rm T}^{-1}$ is the Lorentz contracted factor of the LCMS to PCMS. One can see that the results of $\widetilde{R}'_x$, $\widetilde{R}_y$, and $\widetilde{R}_z$ as functions of $k_{\rm T}$ show a similar trend to that of the HBT radii, although their values are smaller than the corresponding results of the HBT radii. It is well known that the HBT radii obtained by the Gaussian formula fit may be distorted for the sources with non-Gaussian distributions. However, the characteristic sizes of the source given by the first-order moments are model independent [3].

In Fig. 4(d) we exhibit the zero-order moment of the relative coordinate r for the source [3],

$$\widetilde{\lambda} = 4\pi \int_0^\infty \mathrm{d}r S(r) r^2 \,. \tag{15}$$

The value of $\widetilde{\lambda}$ is the intercept of the correlation function at zero relative momentum. Theoretically, it is unity for a completely chaotic source. For comparison, in Fig. 4(h) we show the results of the HBT chaotic parameter λ obtained by the Gaussian formula fit.

In Fig. 5 we show the results of $r_{\sigma R}$, the ratio of the normalized standard deviation $\widetilde{\sigma}$ to the first-order moment $\widetilde{R}$ as functions of k_{T}. Here the symbols $\circ$, $\triangle$, and $\triangledown$ denote $\widetilde{\sigma}_x/\widetilde{R}'_x$, $\widetilde{\sigma}_y/\widetilde{R}_y$, and $\widetilde{\sigma}_z/\widetilde{R}_z$, respectively. One can see that the ratio results in the out direction and in the long direction at the smallest k_{T} are much larger than unity. It is because the corresponding source functions seriously deviate from those of the Gaussian source [3, 22]. The ratio results are consistent with the source functions in Fig. 3. They are sensitive to the shapes of the source functions.

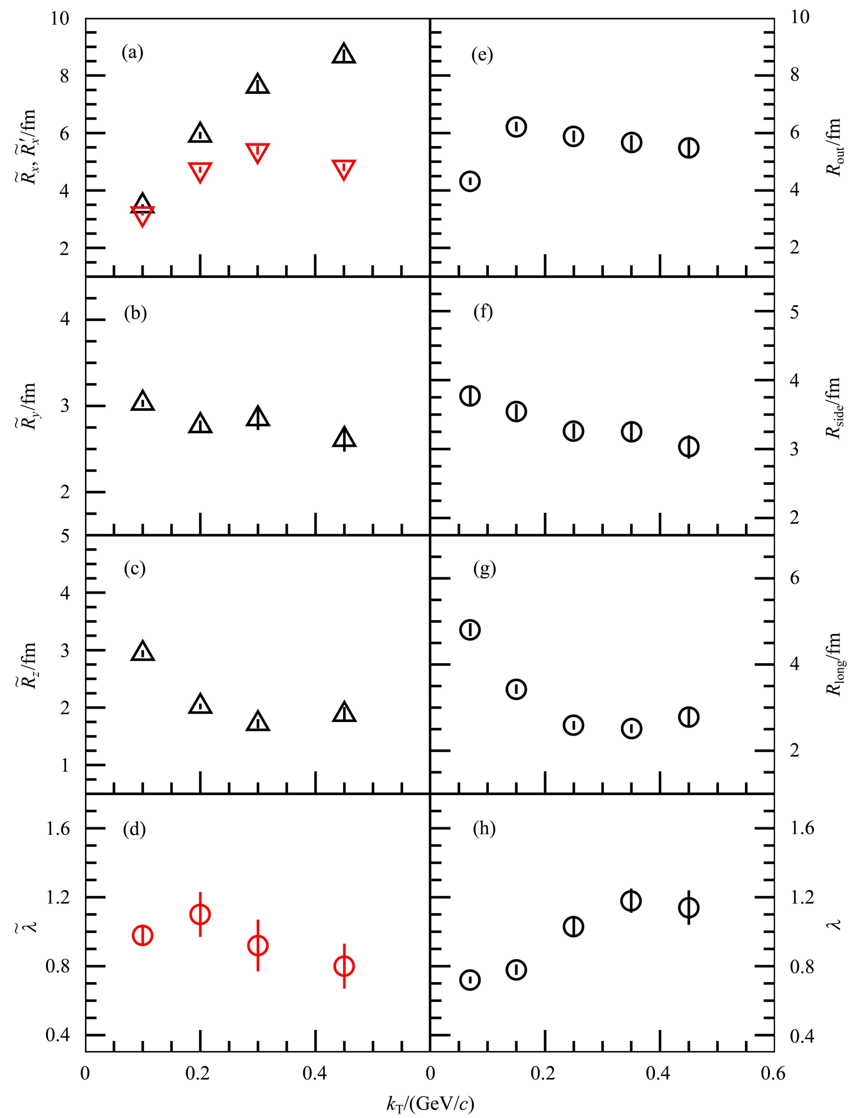

Fig. 4. (a)–(c) The first-order moments in the out, side, and long directions as functions of k_{T}. (d) The zero-order moment as a function of k_{T}. (e)–(g) The HBT radii in the out, side and long directions. (h) The HBT chaotic parameter as a function of k_{T}.

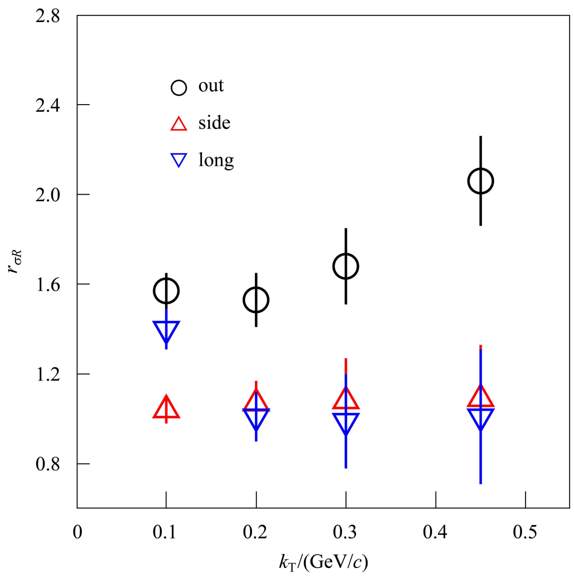

Fig. 5. The ratio of the standard deviation to first-order moment.

4 Summary and conclusion

We investigate the interferometry imaging for the evolving sources in the heavy ion collisions at the HIRFL-CSR energy. The source evolution is described by the relativistic hydrodynamics in (2+1) dimensions. Using the interferometry technique of QTIP [2] and the three-dimension imaging method [19], we investigate the source functions in the out, side and long directions [21]. It is found that the source expansion leads to wide source function distributions in the out and long directions. At a larger transverse pion pair momentum k_{T}, the width of the source function in the out direction is larger than that at smaller k_{T}. However, the width of the source function in the side direction is smaller at larger k_{T} than that at smaller k_{T}. The width of the source function in the long direction is smaller at larger k_{T} because the average longitudinal momentum of the pairs is smaller at larger k_{T}. The investigations for the source function moments indicate that the first-order moments $\widetilde{R}_i$ $(i=x,y,z)$ can describe the source sizes in the out, side and long directions, and the zero-order moment $\widetilde{\lambda}$ may provide information on the chaotic degree of the source. Unlike the HBT results obtained by the usual Gaussian formula fit, the results of the moments are model independent. The ratio of the normalized standard deviation to the first-order moment is sensitive to the shape of the source function. For the non-Gaussian source function, the result of the ratio is larger than unity.

References

1 YU L L, Jirimutu, ZHANG W N et al. Chinese Phys. C (HEP & NP), 2008, **32**: 897
2 YU L L, ZHANG W N, WONG C Y. Phys. Rev. C, 2008, **78**: 014908
3 ZHANG W N, YANG Z T, REN Y Y. Phys. Rev. C, 2009, **80**: 044908
4 Rischke D H, Gyulassy M. Nucl. Phys. A, 1996, **608**: 479
5 Rischke D H. Proceedings of the 11th Chris Engelbrecht Summer School in Theoretical Physics, Cape Town, February 4-13, 1998; nucl-th/9809044
6 Kolb P, Heinz U. nucl-th/0305084
7 Efaaf M J, ZHANG W N, Khalilisar M et al. HEP & NP, 2005, **29**: 46; 467 (in Chinese)
8 Bebie H, Gerber P, Goity J L, Leutwyer H. Nucl. Phys. B, 1992, **378**: 95
9 Hirano T, Tsuda K. Phys. Rev. C, 2002, **66**: 054905
10 Cleymans J, Redlich K. Phys. Rev. Lett., 1998, **81**: 5284
11 XIAO Z G, DONG X, LIU F et al. J. Phys. G, 2007, **34**: 8915
12 Cleymans J, Redlich K. Phys. Rev. C, 1999, **60**: 054908
13 Schneider V et al. J. Comput. Phys., 1993, **105**: 92
14 Rischke D H, Bernard S, Maruhn J A. Nucl. Phys. A, 1995, **595**: 346
15 ZHANG W N, Efaaf M J, WONG C Y. Phys. Rev. C, 2004, **70**: 024903
16 WONG C Y. Introduction to High-Energy Heavy-Ion Collisions. World Scientific, Singapore, 1994. Chap. 17; Wiedemann U A, Heinz U. Phys. Rept., 1999, **319**: 145; Weiner R M. Phys. Rept., 2000, **327**: 249
17 Lisa M A, Pratt S, Soltz R, Wiedemann U. Annu. Rev. Nucl. Part. Sci., 2005, **55**: 357
18 Brown A D, Danielewicz P. Phys. Lett. B, 1997, **398**: 252; Brown A D, Danielewicz P. Phys. Rev. C, 1998, **57**: 2474; Brown A D, Danielewicz P. Phys. Rev. C, 2001, **64**: 014902
19 Danielewicz P, Pratt S. Phys. Lett. B, 2005, **618**: 60; Danielewicz P, Pratt S. Phys. Rev. C, 2007, **75**: 034907
20 Afanasiev S et al. (PHENIX collaboration). Phys. Rev. Lett., 2008, **100**: 232301
21 Bertsch G, Gong M, Tohyama M. Phys. Rev. C, 1986, **37**: 1896; Bertsch G. Nucl. Phys. A, 1989, **498**: 173c; Pratt S, Csörgő T, Zimányi J. Phys. Rev. C, 1990, **42**: 2646
22 YANG Z T, ZHANG W N, HUO L, ZHANG J B. J. Phys. G, 2009, **36**: 015113